Theor Chem Acc (2003) 109:53–63
DOI 10.1007/s00214-002-0394-2

Theoretical
Chemistry Accounts

Feature article

Mechanism and control of molecular energy flow: a modeling perspective

Martin Gruebele

Departments of Chemistry and Physics, Center for Biophysics and Computational Biology, University of Illinois at Urbana-Champaign, Urbana, IL 61801, USA

Received: 26 July 2002 / Accepted: 30 September 2002 / Published online: 2 December 2002

Abstract. Vibrational energy flow in organic molecules occurs by a multiple-time-scale mechanism that can be modeled by a single exponential only in its initial stages. The mechanism is a consequence of the hierarchical structure of the vibrational Hamiltonian, which leads to diffusion of vibrational wavepackets on a manifold with far fewer than the $3N-6$ dimensions of the full vibrational state space. The dynamics are controlled by a local density of states, which does not keep increasing with molecular size. In addition, the number of vibrational coordinates severely perturbed during chemical reaction is small, leading to preservation of the hierarchical structure at chemically interesting energies. This regularity opens up the possibility of controlling chemical reactions by controlling the vibrational energy flow. Computationally, laser control of intramolecular vibrational energy redistribution can be modeled by quantum-classical, or by purely quantum-mechanical models of the molecule and control field.

Keywords: Power law – Coherent control – Symplectic propagator – Quantum diffusion – State space

1 Introduction

The pioneering work of Bixon and Jortner in the 1960s showed that vibrational energy flow (intramolecular vibrational energy redistribution, IVR) must be reckoned with if we are to understand the reactivity of energetically activated molecules [1]. Rapid equipartitioning of a molecule's energy content forms the basis of modern statistical reaction models. The subject of IVR and its effect on chemical reactivity has engendered active interest over the past few decades, with general reviews recapping the theoretical and experimental milestones of the 1970s [2], 1980s [3], and 1990s [4].

As it turns out, IVR is not a totally random process, not even at energies high enough for chemical reaction to occur. The root cause of IVR – vibrational anharmonicity – is relatively weak in organic molecules, thanks to the Born–Oppenheimer separation of electronic and vibrational energy scales [5]. Moreover, the density of states that controls IVR is a local one [6], which depends on the pattern of vibrational resonances resulting from bond connectivity and anharmonicity [7]. Because the local density of states is a function of size-independent molecular properties, IVR does not simply scale with molecular size [8]. Instead, vibrational energy flow is a highly structured process even in large organic molecules. Locally, it can be described by anisotropic diffusion of an initial vibrational wavepacket. Globally, the diffusion occurs on a vibrational manifold of $\delta \ll 3N-6$ dimensions [9]. Even the strongest manifestations of anharmonicity, bond-breaking and bond-making, leave the majority (all but 6) of the vibrational degrees of freedom relatively untouched.

In the modern picture, IVR is pretty efficient at somewhat randomizing molecular energy, but much less efficient at thoroughly randomizing it, even at chemical energies. Anisotropic quantum diffusion, like its classical analogs [2, 10], is a subexponential process. This sluggishness opens up IVR to the possibility of control, and the control of IVR in turn presents a universal mechanism for controlling chemical reactions [8]. My goal here is to summarize these advances from the perspective of quantum-mechanical computational models we have developed to describe the mechanism and control of molecular energy flow, ranging from very specific and accurate molecular models to very general ones based on hierarchical local random matrices. The need for more theoretical work to explain quantitatively the deviations from global statistical behavior observed in reaction

Electronic Supplementary Material to this paper can be obtained by using the Springer Link server located at http://dx.doi.org/10.1007/s00214-002-0394-2.

Correspondence to: M. Gruebele
e-mail: gruebele@scs.uiuc.edu

dynamics experiments already reported in the literature is highlighted in Sect. 5. The reader will find a review of the many other fascinating experimental and theoretical aspects of the subject in the review articles cited in this Introduction, and further articles therein.

2 Hamiltonian and state space model

The coupling structure of the vibrational Hamiltonian, H_{vib}, is hierarchical: when H_{vib} is represented in terms of a set of states localized in some coordinate representation ("feature states"), it can always be brought into a form where an initial state is coupled to a small set of other states, coupled in turn to another small set, and so on. This is in stark contrast to a Hamiltonian with random matrix elements, which cannot be brought into such a form [4]. Feature states are sometimes represented by a tiered tree [11], but a $3N-6$ dimensional state space, with one dimension for each vibrational mode, provides a more complete description (Fig. 1; see also Ref. [4], Fig. 15 for a comparison). In state space, a vibrational wavepacket diffuses on a low-dimensional manifold ($\delta \ll 3N-6$). If δ is less than 1, states are localized, and no energy flow occurs. Above the IVR threshold, vibrational wavepackets still require a very long time to explore the entire state space, but they eventually reach the statistical limit [12]. Exponentially fast exploration of the whole accessible state space would occur only if δ approaches $3N-6$, a limit which is excluded by the local nature of chemical bonding [7]. The origin of this picture is discussed in more detail later.

Within the Born–Oppenheimer approximation, the vibrational Hamiltonian can be written as

$$H_{\mathrm{vib}}/hc = K + \sum_{n=2}^{\infty} \prod_{k=1}^{3N-6} \tilde{V}_{n=\Sigma n_k} \left(a_k^{\dagger} + a_k \right)^{n_k} \qquad (1)$$

in terms of a suitable set of modes $\{k\}$ and their ladder operators. The modes may be normal modes, local modes, or any other reasonably smooth coordinate representation. For our general considerations, the choice does not matter. The kinetic energy, K, is not necessarily quadratic either: appropriate canonical transformations ensure that the anharmonicity has to appear somewhere. In Eq. (1) the potential constants, $\tilde{V}_n$, can be sorted by order $n = \Sigma_k n_k$ equal to 2, 3 (cubic), 4 (quartic), etc.

As a consequence of the separation between electronic and nuclear time scales, each order n has $\tilde{V}_n$ typically smaller by a factor $a = 0.05-0.2$ than the previous order [13]. The factors a_i (not to be confused with the ladder operators a_k) tend to be smaller for lower-frequency modes. Qualitatively, this scaling can be understood as follows. The smaller time scale of electronic motions leads to larger electronic energy level separations: electronic term energies and dissociation energies tend to be 10–100 times larger than vibrational frequencies (20,000 versus 200 cm^{-1}). The change in well curvature with bond distance is affected by the same time scale separation: larger dissociation energies (even faster, lighter electrons) would produce potential wells that curve to dissociation even more gently, thus decreasing the anharmonicity of the potential. Conversely,

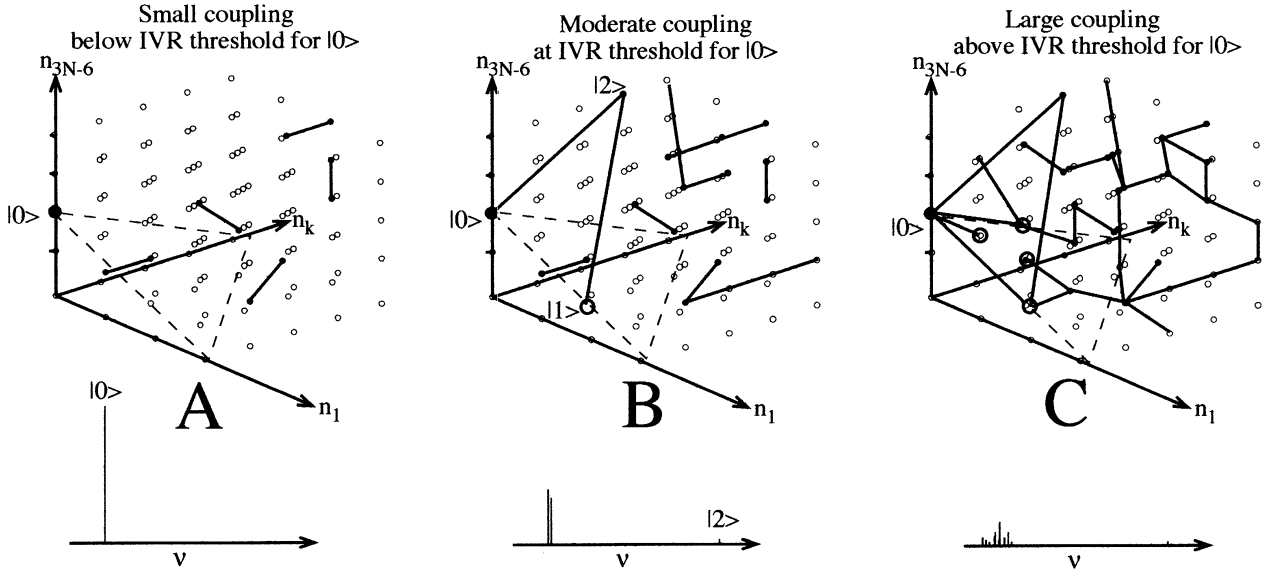

Fig. 1A–C. Vibrational energy flow in state space. Three of the $3N-6$ vibrational quantum number axes are shown, together with the $4 \times 4 \times 5$ cubical lattice of all states from the ground state $|00\cdots0\rangle$to the interior state $|45\cdots5\rangle$. The *thick black lines* indicate significant couplings ($L_{ij} \approx 1$), and the *thin dotted triangle* is a surface of constant vibrational energy. Corresponding intramolecular vibrational energy redistribution (*IVR*) spectra are shown at the bottom. **A** Below the IVR threshold; only isolated resonances exist. **B** Just above the IVR threshold; off-resonant coupling via state $|2\rangle$ lights up two eigenstates in the spectrum that are mixtures of $|0\rangle$ and $|1\rangle$ with no significant admixture of $|2\rangle$, even though $|2\rangle$ mediates the coupling. **C** Well above threshold, direct and higher-order couplings contribute more. From any given point in state space, energy is transported only in a few directions: energy flow is locally anisotropic, and is globally characterized by a dimension $\delta \ll 3N-6$

heavier nuclei produce more closely spaced vibrational levels that lie in the more harmonic part of the surface for a given quantum number n.

This scaling behavior has useful practical consequences. It is remarkable that a sufficiently "random" molecular shape results in potential constants, even for internal rotor modes, that can be represented by a rapidly converging cumulant expansion of the form [7, 14]

$$V_n \approx \prod_{k}^{3N-6} (v_k)^{n_k/n} a_k^{n_k} \prod_{l}^{3N-6} c_{kl}^{(2)n_k n_l} \prod_{m}^{3N-6} c_{klm}^{(3)n_k n_l n_m} \cdots . \qquad (2)$$

The first product term, a fully factorized potential surface, already provides a reasonable approximation for the potential constants of compact molecules. The higher-order terms decrease mode coupling further when modes move different sets of atoms. Except for very high symmetry molecules, coupling constants between vibrational motions of two different atoms drop off exponentially with the number of intervening bonds [7]. Larger organic molecules tend to have fairly low symmetry structures, so most pairs of modes are not strongly directly coupled.[1] For that reason, IVR is governed by a local density of states, which stops increasing above a certain molecular size [6]. The upshot of Eq. (2) is that potential constants generally scale as $\langle v a^{n-3}$ in a predictable way, where n is a cubic or higher order of coupling, and v is a typical cubic coupling constant for a single vibrational mode.

Equations (1) and (2) imply that a limited set of resonant couplings transport energy among modes, as long as the average energy per mode is much less than the electronic energy scale. The latter criterion is satisfied even during chemical reaction, when one or a few out of the $3N-6$ modes approach the electronic energy scale. The resonance structure is best viewed in a $3N-6$ dimensional state space (classically an action space). What states should one pick? Eigenfunctions would be an obvious choice; they render the calculation of dynamics trivial. Unfortunately, Eq. (1) is just sufficiently anharmonic, so the eigenfunctions are hard to evaluate for even modest-size molecules at chemically interesting energies. Instead, it is more useful if we pick a feature basis [46], which is based on the lowest-order terms in the Hamiltonian [1] and includes states that carry oscillator strength. In spirit, this is equivalent to finding the "spectroscopic" Hamiltonian that roughly reproduces the short-time dynamics via anharmonic local, normal, or other simple modes, and then adding couplings among modes, starting with the largest. An objective (but not unique) criterion for choosing feature bases has been given [16].

Figure 1 shows how energy flows in state space. Below the threshold for IVR, only occasional pairs of states are connected by resonances [17]. Just above the threshold, off-resonant couplings are most common, leading to low-order coupling chains that mediate energy flow [18]. In such chains, the couplings between participating states are typically small compared to their energy gaps, and the IVR linewidths are therefore smaller than the couplings [19]. Well above the threshold, direct couplings of increasingly higher order contribute to the dynamics, and the IVR linewidths become larger than the couplings [20]. Because of the local nature of chemical bonding, couplings starting at a given point in state space are not equally strong in all directions. A wavepacket starting at some point generally diffuses in a manifold of dimension much lower than $3N-6$. This leads to a slow decay, $P(t) = |\langle 0|t\rangle|^2$, of the initial state $|0\rangle$, which is closer to a power law, $(1+2kt/\delta)^{-\delta/2}$, than to an exponential decay, e^{-kt}. Only in the limit of $\delta \rightarrow 3N-6$ does the decay $(1+2kt/\delta)^{-\delta/2}$ approach e^{-kt}. It has been shown that δ, as estimated from the energy differences, $\Delta E^{(ij)}$, and couplings, $V^{(ij)}$, among feature states, is in good agreement with full quantum dynamics calculations such as those illustrated in Fig. 2 [16].

Modelling and analysis of experiments have shown that δ is generally much less than $3N-6$: chains of strong resonances spreading in all directions of state space are rare, and the vibrational wavepacket takes a long time before it covers the entire energetically allowed state space. Instead, it must wind its way through a much lower dimensional manifold [12, 16]. Figure 2 shows an experimental decay, $P(t)$, a quantum dynamics simulation based on ab initio calculations, a simulation with a state space molecular mechanics (SSMM) force field (see later) and a quantum dynamics simulation based on a very simple hierarchical local random matrix (HLRM) model that mimics only the most general properties of the molecular Hamiltonian. All four decays are power laws after $P(t) < 0.1-0.01$. They are approximated by a single exponential fit only at early times, and then the golden rule (GR) also provides a good description of the "initial" rate. (The density of states for all the molecules of interest here is large enough that the quantum Zeno effect is negligible, i.e. exponentials provide good fits near but not at $t = 0$.) The two simplest calculations (SSMM and HLRM) merit special emphasis.

SSMM force fields are based on the scaled and factorized potential surfaces given by Eq. (2). They are particularly useful for computing reasonably accurate quantum dynamics of large molecules that are out of the reach of ab initio based methods [12]. Rules for computing potential constants for any type of organic molecule are given in Refs. [5, 7, 14]. The general finding of SSMM quantum dynamics simulations is that large molecules also vibrationally dephase on a manifold whose dimension is much smaller than $3N-6$ [12, 19]. This further suggests that energy flow is governed entirely by the local structure of state space, even in fairly large organic molecules. Analytical models have already shown that the local density of states, not the total density of states, is important for computing IVR properties from the molecular Hamiltonian (see also later) [6, 21], and numerical simulations support this notion [20, 22, 23, 24].

HLRM models can be used to study very general criteria that the Hamiltonian must satisfy to produce

[1] However, very large molecules have a spectral density which remains large below a critical value (about 50–100 cm^{-1}), where extended modes and more delocalized transport are possible. See Ref. [15] for a treatment of proteins segments

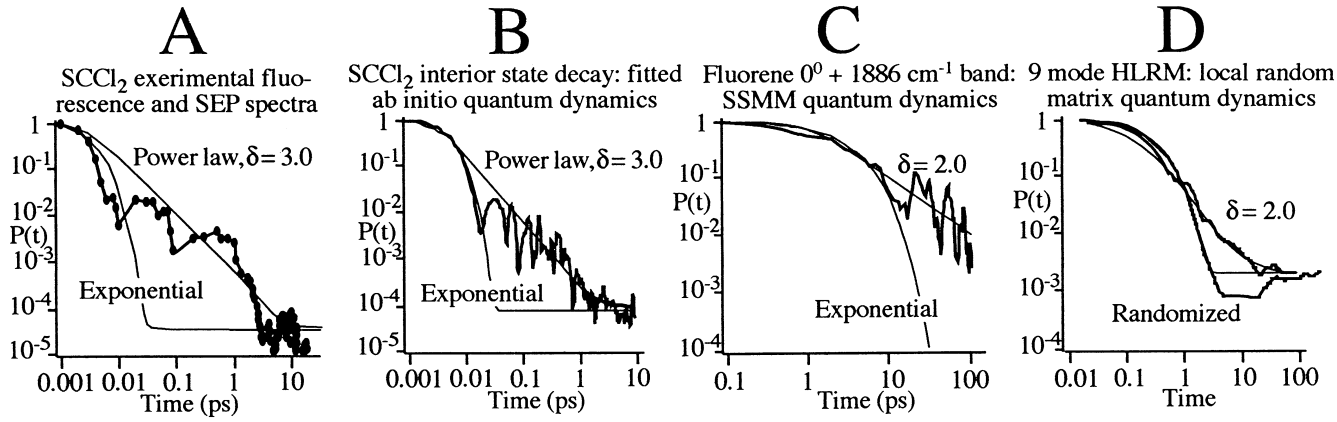

Fig. 2A–D. IVR decays on a log–log scale with exponential and power-law fits shown. **A** Experimental data for $SCCl_2$ [16, 27]. **B** Accurate quantum simulation for an $SCCl_2$ interior state, based on an experimentally refitted ab initio Hamiltonian [16]. **C** State space molecular mechanics calculation for fluorene, showing deviations from exponentiality similar to experiments in a larger molecule [12]. **D** Hierarchical local random matrix calculation with nine degrees of freedom [25]. The "randomized" curve, which fits an exponential with a small coherence hole, is obtained by shuffling the bath–bath couplings of the matrix. Thus, golden-rule-like behavior is reestablished on all time scales when the "triangle rule" correlation among matrix elements is wiped out. Clearly, gateway states (preserved by bath–bath-only shuffling) are not by themselves responsible for the power-law decay

power-law dephasing [25, 26]. The model used in Fig. 2D (dubbed BSTR in Refs. [20, 25]) has only two rules distinguishing it from a global random matrix model.

1. Matrix elements scale as $va^{n^{(ij)}-3}$ with the total quantum number difference, $n^{(ij)} = \Sigma_k n_k^{(ij)}$, between two randomly chosen states $\{i,j\}$.
2. The $n^{(ij)}$ for any triplet of states are subject to the "triangle rule" $|n^{(hi)} - n^{(ij)}| \leq n^{(hj)} \leq |n^{(hi)} + n^{(ij)}|$.

These two rules enforce the same locality of couplings present in a vibrational Hamiltonian: matrix elements drop off exponentially with quantum number difference, and states in a resonant coupled cluster all tend to be coupled to one another, whereas states outside are not. Comparison with ab initio calculations shows that rules 1 and 2 are satisfied by most couplings calculated from potential-energy surfaces. Rules 1 and 2 invariably lead to power-law decays. Interestingly, many other systems with disordered (and hence nonextended) vibrational modes (amorphous solids, liquids at short times, coupled spins in NMR) should obey the same general localization rules [25].

The HLRM highlights the difference between the state space and GR models: if either rule 1 or 2 is relaxed, the IVR dynamics become single-exponential (Fig. 2D). Localized mode couplings are thus essential for a quantitative description of IVR. The single rate constant obtained when rules 1 or 2 are relaxed is identical to the famous GR result $k_{\mathrm{IVR}} = 2\pi/\hbar\rho_{\mathrm{tot}}V_{\mathrm{rms}}^2$, where V_{rms} is the root-mean-square (rms) coupling strength of all prediagonalized "bath" states to the initially prepared state. In practice, V_{rms} cannot be computed without diagonalizing the manifold of bath states, so the GR formula provides no shortcut compared to the state space treatment. Furthermore, the GR expression neglects all correlations between energies and couplings of the bath states, by condensing all the information into one rms coupling strength and one global density of states. In effect, it replaces the local couplings by a mean coupling strength, as though all modes in a molecule were on average equally coupled [4]. Hence the GR prediction that the IVR rate should depend on the global density of states.

3 Some tools for modeling IVR

Many computational tools have been adapted for IVR dynamics. Any calculation must begin by determining an appropriate Hamiltonian. The use of ab initio force fields and SSMM force fields based on Eq. (2) has already been briefly discussed, and a number of examples exist in the literature. When high accuracy is desired, it may be useful to incorporate into ab initio surfaces some experimental information. Scaling all harmonic and anharmonic terms according to Eq. (2) [27] and using potential-shaped interpolation functions [28] are useful tools for generating modified ab initio surfaces that incorporate experimental information. To compute dynamics for a given potential surface, we have developed two approaches, one spectral and one propagator, which have proved very efficient for dealing with IVR problems. These are briefly described.

Symplectic propagators exploit a structural similarity between the time-dependent Schrödinger equation rewritten to split the real and imaginary parts into two components of a vector [29],

$$\begin{pmatrix} \mathrm{Re}(\dot{\Psi}) \\ \mathrm{Im}(\dot{\Psi}) \end{pmatrix} = \begin{pmatrix} 0 & -\hat{H} \\ \hat{H} & 0 \end{pmatrix} \begin{pmatrix} \mathrm{Re}(\Psi) \\ \mathrm{Im}(\Psi) \end{pmatrix} , \tag{3}$$

and Hamilton's equations of motion. We developed the simplest of these, the "shifted-update-rotation" propagator or SUR, specifically for IVR calculations [30]. It requires only a few lines of code and minimal variable storage. Its quadratic phase convergence makes it possible to tailor the accumulated error, so calculations

can run for 10–100 ps with 10^4–10^6 basis states and less than 1% rms error, before propagators with linear scaling and sudden error onset as a function of time step, such as the Chebyshev propagator [31], become more efficient. This is particularly attractive when large families of shorter calculations are required, such as when looking at the statistical ensemble dynamics of HLRM models [25]. The results of the calculations shown in Fig. 2B–D were carried out with the SUR propagator. In addition, variants of the SUR propagator are fast and robust in the presence of time-varying matrix elements, and have been used to compute IVR in the presence of electromagnetic fields pumping molecular transitions, for example, in quantum-classical control calculations [32].

When eigenstate resolution is desired, spectral methods for calculating IVR lineshapes are useful [33, 34, 35, 36]. The generic problem is summarized in Fig. 3. An initial state $|0\rangle$ is coupled to a bath manifold $\{|i\rangle\}$, which is usually not prediagonalized. In principle, diagonalizing the Hamiltonian yields the eigenstates $|n\rangle$, line positions E_n, and intensities $|\langle n|0\rangle|^2$. The difficulty with the IVR Hamiltonian is that it requires many basis states, even in the discrete variable representation [37], which improves the sparseness, but not the size, of the Hamiltonian. The eigenvectors are not very sparse above the IVR threshold, and must be computed at great expense to extract intensities. For matrix sizes exceeding $10^4 \times 10^4$ the expense rapidly becomes prohibitive.

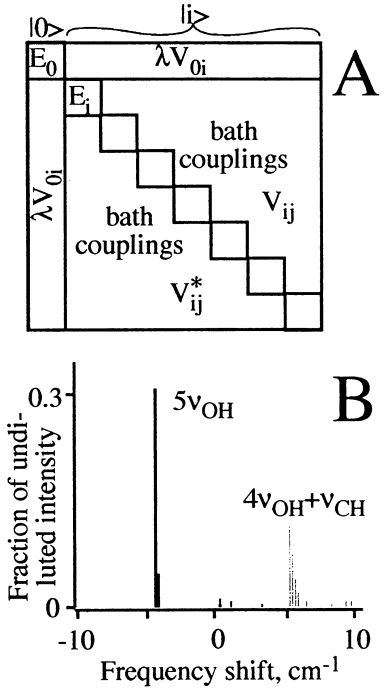

Fig. 3. A Setup of the IVR Hamiltonian for the matrix fluctuation dissipation (*MFD*) theorem. λ multiplies only the off-diagonal elements connecting the "bright" state to the bath. **B** Large-scale BSTR-MFD quantum calculation of IVR in the fourth OH overtone region of methanol; the overtone and combination band are strongly coupled, but differently broadened because of fluctuations in the "bath" local density of states [24]

The matrix fluctuation dissipation (MFD) theorem is one solution to this problem. If we imagine that the off-diagonal matrix elements coupling the initial state to the bath manifold are scaled by a unitless parameter $\lambda \approx 1$, then one can use the Hellmann–Feynman theorem to prove that [35, 38]

$$|\langle n|0\rangle|^2 = \left.\frac{\partial \ln E_n}{\partial \lambda}\right|_{\lambda=1} \tag{4}$$

if $\mathrm{Tr}\{H\} = 0$ (i.e. the line center is shifted to zero energy). Variations on Eq. (4) are possible by scaling other matrix elements of H, but they always relate the line intensities to derivatives of the eigenvalues. This means that the lineshape (and hence rate) can be calculated via two eigenvalue evaluations, without explicit knowledge of the eigenstates. Practical implementations of the MFD theorem often use Lanczos iteration, and in that way are analogous to "recursive residue generation" [33], although Eq. (4) is a nonrecursive relation for the spectral intensities.

Figure 3 shows an IVR line shape calculated for the fourth OH stretching overtone of methanol using the MFD theorem and a SSMM potential surface [24]. Such a simple potential cannot be expected to agree exactly with experiment, but it shows the same qualitative features [39]: the $4\nu_{CH} + \nu_{OH}$ overtone borrows intensity from $5\nu_{OH}$, and shows a different local IVR rate (feature width). The MFD theorem has been used for calculations ranging from accurate potential surfaces to HLRMs [12, 20, 25]. It has recently been adapted for a fully quantum mechanical control theory which can be used to study IVR (Sect. 6) [40], and Chen and Guo [41] have used it to automatically assign quantum numbers based on coordinate operator matrix elements.

4 What the models tell us

One of the most fundamental concepts in the state space theory of IVR is the local number of coupled states, N_{loc} [4]. By binning the local coupled states into fixed energy intervals, one obtains the local density of states, ρ_{loc}. N_{loc} near state j is given by

$$N_{loc} = \Sigma_i L_{ij}^2 \,, \tag{5}$$

where one approximates with reasonable accuracy $L_{ij} \approx 1/\sqrt{1 + (\Delta E^{(ij)}/V^{(ij)})^2}$. [7]. The energy gaps and coupling matrix elements depend sensitively on bonding, and can be calculated from potential surfaces ranging from ab initio to SSMM to local random matrix, depending on the size of the system and the computational power available.

Another important quantity is the effective number of participating states, N_{eff}. If an initially prepared vibrational wavepacket dephases over a total of N_{eff} states, its survival probability $P(t)$ will be diluted from 1 (at $t = 0$) to the "dilution factor" $\sigma = N_{eff}^{-1}$ [42]. For example, if $P(t)$ drops to 0.001, this indicates that 1,000 states are participating in the IVR. If all states are populated, on average, the same as $t \to \infty$, then the statistical share of the initial state becomes the observed 0.001. N_{eff} can be

computed from the IVR lineshape, or measured experimentally from the decay $P(t)$ or from high resolution spectra. N_{eff} is generally larger than N_{loc}: the local neighbors of the bright state will show up in the spectrum, but with lower intensity so will the neighbor's local neighbors, and so forth.

The relationship between these fundamental quantities for many small organic molecules is shown in Fig. 4. N_{eff} was measured experimentally by Stewart and McDonald [42]. The range of predictions from the BSTR local random matrix model is also shown in Fig. 4, and is in excellent agreement with experiment. When N_{loc} exceeds 1, N_{eff} rapidly increases to the total number of eigenstates under the IVR lineshape; below the threshold, $N_{\text{eff}} \rightarrow 1$ and no energy redistribution occurs. This threshold behavior occurs as the transition from Fig. 1A to b is made. A similar plot against the total density of states shows only a weak correlation, and only because the molecules studied were mostly smaller than the average localization length of a vibrational mode (usually 2–3 bonds).

An early success for the local density of states model was the prediction of the broadening mechanism for strongly coupled Darling–Dennison resonant state pairs in methanol [24]. Boyarkin et al. [39] found experimentally that the $4\nu_{\text{CH}} + \nu_{\text{OH}}$ band borrows intensity from the $5\nu_{\text{OH}}$ overtone, to the point where both transitions are nearly equally intense. Yet despite the strong coupling, their linewidths are very different. Symmetry arguments (plus/minus combination of dark and bright states have different phases) and fluctuations in the local density of bath states, which couple differently to interior and edge states (Fig. 1), were put forth as hypotheses. Our large-scale local random matrix simulations came out in favor of the latter, predicting that the combination band would be more fragmented in 80% of the cases and the pure overtone (edge state) in 20% of the cases (see the example in Fig. 3). Later experiments with ^{13}C methanol confirmed that the dilution factor of the narrower band could be increased relative to the other by shifting the bands on top of different bath states [43]. Clearly, nearly isoenergetic, strongly coupled spectral features can have very different IVR rates, which is best explained in terms of fluctuations in the small local density of states.

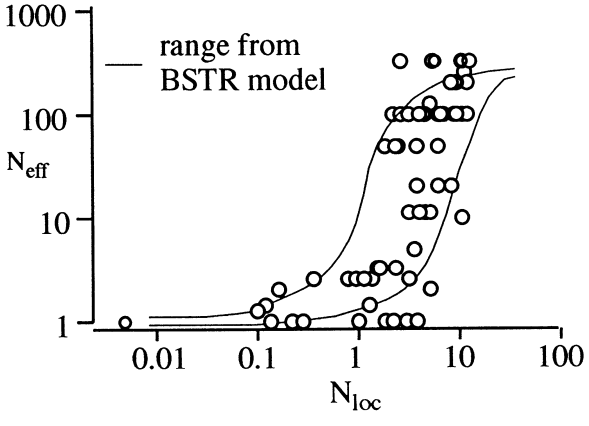

Fig. 4. Correlation of effective number of participating states with local number of coupled states. Above the IVR threshold at $N_{\text{loc}} \approx 1$, N_{eff} rapidly increases and the initially prepared state is diluted over many eigenstates. The *circles* are reanalyzed experimental data from Ref. [42], the *thin lines* are the range predicted by the BSTR model [23]

Recently, IVR computations in the threshold region of organic molecules with ten or more atoms have become possible [19]. Calculations based on Hartree–Fock potential surfaces are too harmonic, but a uniform rescaling of the anharmonicity, so that vibrational frequencies agree with experiment, also brings the IVR linewidths and N_{eff} into agreement with experiment. Calculations for pyrrole and triazine reveal the mechanism shown in Fig. 2B. The IVR linewidths are much narrower than the off-resonant couplings that give rise to them. The calculations also explain why most of the gateway states that mediate the effective coupling of nearly isoenergetic states remain invisible in the spectrum (a quantum phase interference effect) [19].

Another important effect of localization is the competition between more coupling partners available for "interior" states in state space versus stronger local couplings for "edge" states. Interior states are those deeply embedded in state space (Fig. 1), with many modes excited simultaneously; this is the more common kind of state. Edge states include overtones with excitation in only one mode; these are the optically more accessible states. Experiments and simulations of the seven-atom molecule propyne (H_3C-C≡C-H) show that the concentration of energy in a single edge state can lead to more IVR [22, 24, 44, 45]. The acetylenic CH stretching overtone $3\nu_1$ has a larger N_{eff} than the nearly isoenergetic methyl stretch/acetylenic stretch combination band $2\nu_1 + \nu_6$. This is best pictured as follows. The combination band distributes the energy into two packets, localized at opposite ends of the molecule. The resulting local densities of states mimic separate low-energy $2\nu_1$ and ν_6 excitation. Overtone excitation deposits the full energy in one spot, yielding a higher local density of states. In sufficiently large molecules, one would generally expect excitation of two nonoverlapping modes to result in less IVR than the same energy being concentrated in one mode. For ring structures, for localized but overlapping modes moving the same atoms, or for delocalized modes, the larger number of potential coupling partners in the interior of state space would win out.

Calculations of initial IVR decay rates based on state space models generally give good agreement with experimental data [12, 22]. Of more interest with regard to nonstatistical reactions and control of IVR is the subsequent power-law decay of IVR predicted by the state space calculations [9, 12, 22]. The most detailed experimental and quantum dynamics study to date is for the six degree of freedom system thiophosgene [16, 27]. Stimulated emission pumping vibrational spectra from the zero point to the dissociation limit show at least four layers of hierarchical structure. (The top layer is generally termed "polyad structure", on the basis of the extensive acetylene studies reviewed by Nesbitt and Field [46]). Calculations of δ, both by analysis of the resonant coupling structure and by quantum dynamics calcula-

tions on a fitted high level ab initio surface, yield $\delta \approx 3$ for interior states at 9,500 cm^{-1}. Isoenergetic edge states, such as the $7\nu_{CS}$ stretching overtone have $\delta \approx 1$, and lie just at the localization transition [16]. If we imagined the entire vibrational spectrum excited by an ultrafast laser, completion of the IVR process is delayed by 2 orders of magnitude in time (Fig. 2A), from the femtossecond into the picosecond region.

SSMM analysis and quantum simulations on the much larger fluorene and cyclohexylaniline molecules [12], studied experimentally by Kauffman et al. [47] and Smith and McDonald [48], show a similar picture, with δ in the range 1–4 depending on the part of state space initially accessed. Again, the completion of the IVR process is delayed by orders of magnitude in time. Very recent work by Pate and coworkers [49, B.H. Pate personal communication] on substituted alcohols, using microwave–IR multiresonance methods to access the decay of both bright and bath states, also verifies the multiple time scale behavior. Although their data is presently accounted for by a biexponential decay, further probing is likely to reveal additional time scales.

Many more examples of the application of state space models to IVR exist, but the ones already described provide a flavor of the differences between local and global modeling of IVR. Experiment and modeling agree that the extent and time course of IVR require models that take into account the local nature of chemical bonding, and hence the highly directional structure of vibrational resonances in state space. The next questions are: what does this have to do with chemical reactivity, and can we use the local nature of IVR to control reactivity?

5 Is statistical reactivity only "skin-deep"?

Statistical rate models such as the Rice–Rampsberger–Kassel–Marcus (RRKM) model have enjoyed enormous success. In many experiments, preparation is statistical to begin with, and IVR is not necessary to ensure a statistical outcome [50]. Even with quantum state-specific preparation, IVR – asymptotic dynamics notwithstanding – generally provides sufficiently fast randomization of an evolving vibrational wavepacket, so reactivity can be estimated based on an equipartitioning of energy among vibrational modes. Still, this begs the question: is the outcome statistical by a wide margin, or is IVR just barely fast enough when initial states are carefully prepared? The latter makes for many interesting possibilities of controlling reaction dynamics. Indeed, there are numerous subtle experimental examples of large-molecule nonstatistical behavior, indicating that the statistical description fails when we dig deeper into the underlying dynamics. Such nonstatistical properties "just below the skin" could be exploited by the IVR control mechanisms discussed in Sect. 6.

Deviations from statistical rate theory for triatomic molecules, van der Waals clusters, and reactions proceeding on directly dissociative surfaces have been well documented. A particularly important mechanism in such cases is short-time passage via direct paths: a fraction of the molecular wavepacket reacts immediately before the onset of IVR [51]. Here we discuss experimental and computational examples of the deviations that occur in larger organic molecules reacting on bound potential wells. The reason for this choice is simply that those molecules are chemically the vast majority of interesting subjects for reaction control. Although the discrepancies from statistical expectations are subtler, so one could plead a special case for each example, they are pervasive.

Many experiments document irregularities in the isotope dependence of reaction rates. For example, the electronically excited dissociation of acetone studied by Owrutsky and Baronavski [52] deviates from RRKM predictions: no decrease in dissociation rate upon deuteration is observed. SSMM calculations for ground-state acetone show that it has a very small local density of states even several thousand reciprocal centimeters above the zero point level [23]. An even more dramatic example is the cis–trans isomerization of stilbene, either doubly deuterated at the two vinyl positions or tenfold deuterated on the phenyl rings [53].The d_2 compound with the lower total density of states reacts more slowly than the d_{10} compound. These measurements indicate that the rate is not controlled by the total density of states, but rather by the local number of coupled states, N_{loc}, because of incomplete IVR. A simple IVR-isomerization model, which could explain such behavior, and which also explains the anomalous pressure dependence of the isomerization rate, has been proposed on the basis of SSMM force field calculations [54]. Purely statistical discussions of stilbene isomerization, although capable of explaining many general trends, are forced to selectively dismiss or ignore isotopic and pressure-dependent data [55].

Subtler isotope effects also exist for heavier atoms. Hathorn and Marcus [56] studied in detail nonstatistical bimolecular isotopomer production of ozone from oxygen molecules and atoms. The non-RRKM effect is small (15%), but indicates again that energy flow in the state space is partitioned or locally anisotropic. As is often the case, the deviation from statistical theory is not dramatic, but indicates that incomplete energy flow lurks just below the surface of thermally averaged observations. Studies of IVR rates themselves, of course, support the notion of a local density of states as the important parameter, as discussed in Sect. 4.

A very recent example of nonstatistical isomerization in a large molecule involves the population of conformers of *N*-acetyl-tryptophan methyl amide by Dian et al. [57]. Excitation of different NH fundamentals leads to very different distributions of nearly isoenergetic conformers. This result is puzzling in the context of total density of states models, but it might be explainable, if the conformer local densities of states are sufficiently different. Like the cyclohexylaniline and methanol IVR discussed in Sect. 4, the local density of states can fluctuate significantly even in large molecules because it depends only weakly on size, and depends instead on the local bonding patterns.

As a final example, the threshold dependence of nonstatistical behavior is of particular interest from the point of view of IVR control. Osterheld and Brauman [58] investigated nonstatistical product formation in the isomerization reaction of acetone enol cation to acetone ion with subsequent loss of methyl groups. They found that the product formation becomes increasingly nonstatistical, as the threshold for enol–acetone isomerization is exceeded. Multiple time scales of IVR in the state space model offer a general explanation for such behavior. Near the reaction threshold, reaction times usually lie in the (sub)nanosecond range, giving even power-law IVR enough time to reach the statistical limit. A few thousand reciprocal centimeters above the threshold, the reaction rates increase from the reciprocal nanosecond to the reciprocal picosecond range [59], while IVR remains nearly unchanged. The reacting molecule now samples the power-law tail of incomplete IVR, allowing the initial state to manifest itself in the transition-state dynamics. In effect, the reaction dynamics time scale is tuning through the multiple IVR time scales as a function of energy above threshold.[2]

All these examples indicate that energy flow does a passable job at randomizing vibrational wavepackets near the thermal threshold. However, on moving up in energy into the realm of above-threshold photochemistry, slower IVR time scales could manifest themselves as the reaction dynamics speed up. Clearly, much theoretical work remains to be done, considering that most of the experimental examples discussed here have not been subject to a detailed quantitative explanation.

6 Quantum-classical and quantum control of IVR

The quest to control chemical reactions with lasers [60] is as old as the quest to understand IVR, and is intimately connected with it [8]. In highly excited organic molecules, vibrational and vibronic couplings are the strongest coherence-loss mechanisms. Expensive mode-specifically deposited laser energy tends to flow throughout the molecule, and one might as well have used a heating mantle to achieve the same result.

At least this is how things appear on the surface. A closer look, as taken in Sects. 2, 3, 4, and 5, shows that this picture may be correct after tens of picoseconds, but not necessarily before that. The initial IVR decay (Fig. 2) is sufficient to randomize the reacting wavepacket superficially, but then the decay plateaus into a power law. The meaning of "superficial" is illustrated in Fig. 5. where N_{eff} is plotted as a function of time during the evolution of the vibrational wavepacket. The curve starts out at 1, then increases to astronomical values in large molecules. However, anisotropic quantum diffusion in state space is a much slower than exponential process, and increasingly lengthy time spans are required to reach

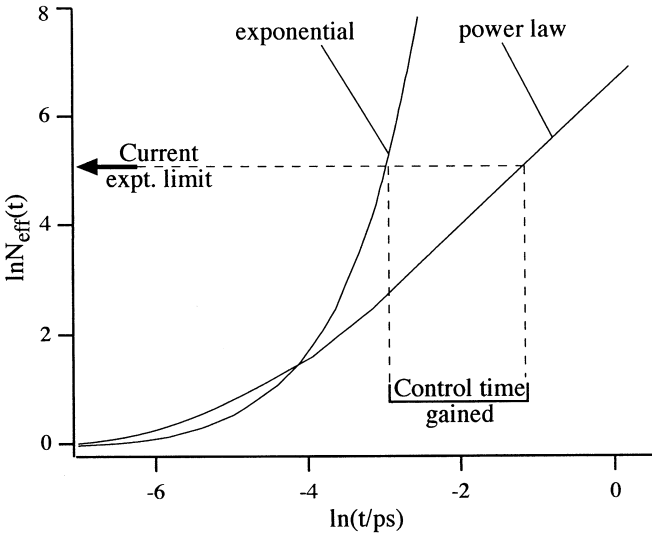

Fig. 5. Power-law dynamics greatly extends the temporal range over which a given number of control parameters can control the dynamics, when compared to exponential dynamics [32]

the last expanses of state space. Now we have an issue of controllability: how many states N_{eff} can one control? Modern laser pulse-shaping equipment is approaching 1,000 channels of complete frequency and phase control; therefore any decay of the wavepacket survival probability up to 0.001 is "superficial", and can be reversed as a matter of principle. As indicated in Fig. 5, this can buy 1–3 orders of magnitude in time, depending on the exact values of k_{IVR} and δ [32]. The difference between exponential and power-law decays is not merely cosmetic, but qualitative: further progress in control capability buys very little time along an exponential decay, but potentially a lot along a power-law decay.

The concept of "irreversible" IVR of large molecules must be made more precise now. As long as N_{eff} is smaller than the number of energy/phase control channels in available pulse shapers, the IVR decay is reversible in principle. Only when that number is exceeded does the IVR decay become irreversible. Modest advances in control capability can push the irreversible time scale back significantly when the decay is not exponentially fast.

Because the initial stages of IVR at chemical energies generally occur on a time scale greater than 50 fs, control over an additional 2 orders of magnitude in time is sufficient to reach the reaction time scale. No control is required beyond that, so coherence needs to be maintained only over an energy window $\Delta E \approx \hbar/\tau_{\text{rx}}$. This immediately suggests the following control scheme: use coherent laser control to "freeze" the IVR for as long as possible, and tailor product formation by selecting different initial states which are coupled to different parts of the reactive continuum [8]. When IVR is "frozen", reaction via direct paths (Sect. 5) is introduced in larger molecules, by reducing the effectiveness of the competing IVR channel. Such a mechanism would allow coherent control of reactivity, but could also be important in strong-field control: a weaker prepulse affecting energy

[2] Vibronic couplings complicate the picture; however, most molecules are not as exotic as the visible/near-UV absorbers and dyes favored by laser spectroscopists, and major vibronic effects on the ground-state surface are usually limited to isolated functional groups.

flow could bias the molecule toward certain channels before field strengths comparable to Coulomb interactions rip the molecule apart.

Is IVR control possible in practice? This can be addressed by quantum calculations, which can be grouped into two classes:

1. In the familiar quantum-classical models, the relevant Hamiltonian is $\hat{H} = \hat{H}_{\mathrm{mol}} - \hat{\mu}E(t)$, and the laser field is treated as a classical variable.
2. Recently, a full quantum model has been developed, which yields surprisingly simple and manageable exact control functional.

We discuss these approaches in turn.

A classical pulse-shaped control field that increases the100-fs initial decay rate of the $8\nu_{\mathrm{CS}}$ stretching state of thiophosgene to about 7 ps is shown in Fig. 6. The computations were performed with a 6D SSMM Hamiltonian using the SUR propagator [32]. The electric field was represented by a wavelet transform to allow simultaneous optimization on all frequency scales, and simulated annealing was used for the feedback optimization. A modest 64 control channels and 80-fs input pulse were used in the calculation, both within reach of experiments, which currently could be scaled to 1,000 channels per 10-fs input pulse. Rotational dephasing in this molecule (and in all molecules large enough to be interesting to control) occurs only on a time scale greater than 10 ps. Thus freezing of IVR is a practical possibility [8].

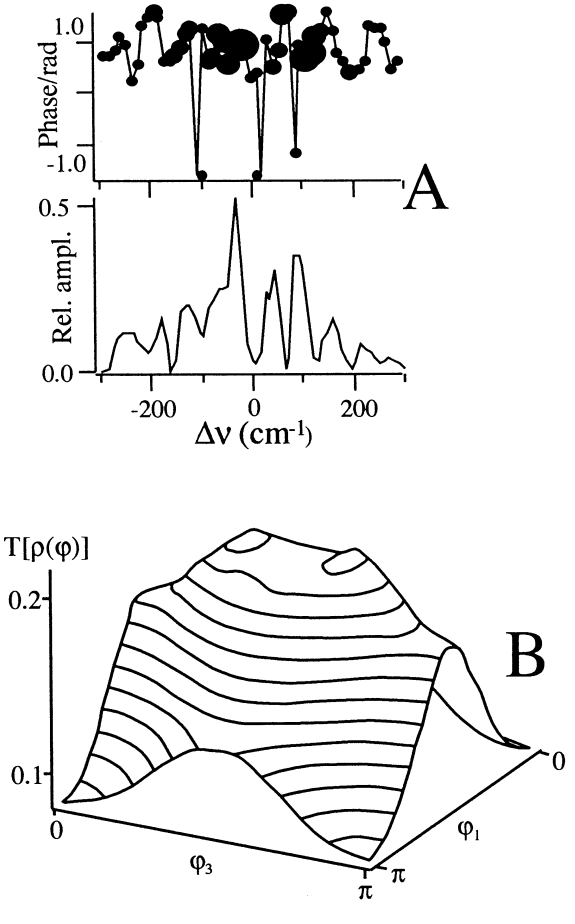

Fig. 6. **A** Control field freezes the initial IVR decay of the seventh CS overtone of thiophosgene by 2 orders of magnitude longer than the "natural" IVR decay excited by an 80-fs Gaussian pulse. Control phase and amplitude from Ref. [32]. The *largest black circles* indicate the phases associated with the largest amplitudes. **B** Full quantum control calculation for two reactive states coupled by three IVR states that induce dephasing [40]. A 2D slice through the amplitude-phase control surface is shown

In full quantum control, the laser is treated as a quantum field, and the exact control Hamiltonian has the form

$$H = H_{\mathrm{mol}} + \sum_i \hbar\omega_i \left(a_i^\dagger a_i + \frac{1}{2} \right) - \sum_{n,i} c_{ni} \hat{\mu}_n \left(a_i^\dagger + a_i \right) + H_{\mathrm{int}}^{(2)} \,. \tag{5}$$

For simplicity, the field polarization and **k** vectors have been lumped into one index i per mode, the nonrelativistic approximation is made, the dipole approximation is made, and $H^{(2)}$, a further correction to the interaction Hamiltonian in the strong-field limit, is not given explicitly. None of these simplifications affect the generality of this discussion. The full quantum Hamiltonian has two important advantages [40]. First, H is time-independent, greatly simplifying the quantum dynamics. Second, H does not depend on the control parameters, which are now encoded in the molecule-field density matrix. In principle, the control problem can therefore be solved by noniterative linear variational techniques.

Consider, for example, the target optimization functional

$$T[\rho(\mathbf{c})] = \int_{-\infty}^{\infty} \mathrm{d}t \, \mathrm{Tr}\{\rho_{\mathrm{T}}(\mathbf{c}) \exp(-iHt/\hbar) \times \rho_0(\mathbf{c}) \exp(iHt/\hbar)\}. \tag{6}$$

The initial system-field density operator, ρ_0, is propagated in time, overlapped with the target, ρ_{T}, and this overlap is maximized. The optimization parameters, **c**, do not occur in the exponential and H is time-independent, so the whole expression can be integrated analytically to yield in the simplest case (see supplementary material) [40]

$$T[\mathbf{c}] \sim \sum_N \frac{\partial E_N[\mathbf{c}]}{\partial \lambda} \frac{\partial E_N[\mathbf{c}]}{\partial \lambda'} \,, \tag{7}$$

where E_{N} are eigenvalues of the operator $\hat{O} = \hat{H} + \lambda\hat{\rho}_0 + \lambda'\hat{\rho}_{\mathrm{T}}$ (no knowledge of the eigenstates of $\hat{O}$ is required). Equation (7) is completely symmetrical, and can also be used to study the output field after interaction. This possibility is of particular interest because phase/amplitude wavefront detection of optical pulses is becoming feasible, opening up the possibility of new types of linear and nonlinear spectroscopies, where the full output field distribution is analyzed (most current experiments just analyze an output intensity). It has been shown that the same techniques used to filter state space basis sets

for IVR can also be used to filter the molecule-field basis to a manageable size, and computational examples of Eq. (7) are given in Ref. [40]. Figure 6 shows an example where the population of two isoenergetic product states is tuned by coherently exciting an IVR "toy" manifold of three states that provide dephasing.

Two additional aspects of Eqs. (5), (6), and (7) will be discussed here. As written in Eq. (6), the density matrices subject to optimization are for the field and molecule. This is useful if one wants to incorporate explicit constraints in the field, or in the strong-field limit, when molecular states are no longer independently defined. In weak-field control, one often wishes to optimize just a particular set of molecular states, for example, to freeze IVR. This can be achieved easily by choosing a target density matrix of the type

$$\rho_{\mathrm{T}} = \begin{pmatrix} 0 & & 0 & & 0 \\ & \begin{pmatrix} 1/N & 0 & 0 \\ 0 & \ddots & 0 \\ 0 & 0 & 1/N \end{pmatrix} & & 0 & \\ 0 & & & & \\ & & 0 & & 0 \end{pmatrix}. \tag{8}$$

This matrix is organized into blocks corresponding to one molecular state each (but many field states). Only one molecular state block is nonzero, projecting the total density matrix onto the desired system state irrespective of the resulting field states.

Equation (5) suggests an even more powerful future approach to the full quantum control problem, which could provide an exact solution for the functional [7]. The quantum field Hamiltonian consists of a set of uncoupled harmonic oscillators, coupled linearly to the molecule. The influence of such a boson bath on a molecule can be evaluated exactly via path integrals [61]. Current path integral techniques are pushing towards larger H_{mol}, and calculations with multilevel molecules relevant to IVR control may soon be within computational reach.

The kinds of IVR control schemes restricting energy flow described here may already be operative in coherent control experiments of larger molecules such as iron carbonyls [62] or organic ions [63]. Currently, these systems are treated as "black boxes" subject to optimization [60]. Systematic variation of molecules to tailor their local density of states could reveal how much a reduction of IVR is responsible for the observed control.

7 Outlook

Subtle deviations in reaction dynamics experiments indicate that chemical reactivity, particularly photochemical, is not within the statistical territory by many orders of magnitude. Locally anisotropic diffusion of vibrational wavepackets in state space on multiple time scales provides a natural description for these deviations. The power-law tail of IVR decays allows vibrational energy flow to be frozen over interestingly long time scales, possibly extending the regime of nonstatistical reactivity. Future calculation should try to account for these subtle deviations from fully statistical behavior. Future experiments should investigate systematically whether chemical reactions in large molecules can indeed be controlled by optically freezing molecular energy flow.

Acknowledgement. This work was supported by NSF grant CHE 9986670.

References

1. Bixon M, Jortner J (1968) J Chem Phys 48: 715
2. Rice SA (1981) Adv Chem Phys 47: 117
3. Uzer T (1991) Phys Rep 199: 73
4. Gruebele M (2000) Adv Chem Phys 114: 193
5. Madsen D, Pearman R, Gruebele M (1997) J Chem Phys 106: 5874
6. Logan DE, Wolynes PG (1990) J Chem Phys 93: 4994
7. Pearman R, Gruebele M (1998) J Chem Phys 108: 6561
8. Gruebele M, Bigwood R (1998) Int Rev Phys Chem 17: 91
9. Schofield S, Wolynes PG (1993) J Chem Phys 98: 1123
10. Kuz'min MV, Nemov IV, Stuchebrukhov AA, Bagratashvili VN, Letokhov VS (1986) Chem Phys Lett 124: 522
11. Quack M (1983) Faraday Discuss Chem Soc 75: 359
12. Gruebele M (1998) Proc Natl Acad Sci USA 95: 5965
13. Oka T (1967) J Chem Phys 47: 5410
14. Pearman R, Gruebele M (2000) Z Phys Chem 214: 1439
15. Leitner D (2001) Phys Rev Lett 87: 188102
16. Wong V, Gruebele M (1999) J Phys Chem 103: 10083
17. Stuchebrukhov AA, Kuzmin MV, Bagratashvili VN, Lethokov VS (1986) Chem Phys 107: 429
18. Stuchebrukhov AA, Mehta A, Marcus RA (1993) J Phys Chem 97: 12491
19. Callegari A, Pearman R, Choi S, Engels P, Srivastava H, Gruebele M, Lehmann KK, Scoles G (2002) Mol Phys (in press)
20. Gruebele M (1996) J Phys Chem 100: 12183
21. Leitner DM, Wolynes PG (1996) Chem Phys Lett 258: 18
22. Bigwood R, Gruebele M (1995) Chem Phys Lett 235: 604
23. Bigwood R, Gruebele M, Leitner DM, Wolynes PG (1998) Proc Natl Acad Sci USA 95: 5960
24. Bigwood R, Gruebele M (1997) ACH Model Chem 134: 675
25. Wong V, Gruebele M (2001) Phys Rev A 63: 22502
26. Wong V, Gruebele M (2002) Chem Phys 284: 29
27. Bigwood R, Milam B, Gruebele M (1998) Chem Phys Lett 287: 333
28. Strickler B, Gruebele M (2001) Chem Phys Lett 349: 137
29. Gray SK, Verosky JM (1994) J Chem Phys 100: 5011
30. Bigwood R, Gruebele M (1995) Chem Phys Lett 233: 383
31. Tal-Ezer H, Kosloff R (1984) J Chem Phys 81: 3967
32. Bigwood RM, Gruebele M (2002) J Mol Struct (THEOCHEM) 589: 447
33. Wyatt RE (1989) Adv Chem Phys 73: 231
34. Huang SW, Carrington T (2000) J Chem Phys 112: 8765
35. Gruebele M (1996) J Chem Phys 104: 2453
36. Mandelshtam VA, Taylor HS (1997) J Chem Phys 107: 6756
37. Light JC, Hamilton IP, Lill JV (1985) J Chem Phys 82: 1400
38. Gruebele M (1996) J Phys Chem 100: 12178
39. Boyarkin OV, Lubich L, Settle RDF, Perry DS, Rizzo TR (1997) J Chem Phys 107: 8409
40. Gruebele M (2001) Chem Phys 267: 33
41. Chen R, Guo H (1999) Chem Phys Lett 308: 123
42. Stewart GM, McDonald JD (1983) J Chem Phys 78: 3907
43. Chirokolava A, Perry DS, Boyarkin OV, Schmid M, Rizzo TR (2000) J Chem Phys 113: 10068
44. Gambogi JE, Timmermans JH, Lehmann KK, Scoles G (1993) J Chem Phys 99: 9314
45. Lehmann KK, Scoles G, Pate BH (1994) Annu Rev Phys Chem 45: 241
46. Nesbitt DJ, Field RW (1996) J Phys Chem 100: 12735
47. Kauffman JF, Coté MJ, Smith PG, McDonald JD (1989) J Chem Phys 90: 2874

48. Smith PG, McDonald JD (1990) J Chem Phys 92: 1004
49. Keske JC, Pate BH (2000) Annu Rev Phys Chem 51: 323
50. Miller WH (1987) Chem Rev 87: 19
51. Remacle F, Levine RD (1991) J Phys Chem 95: 7124
52. Owrutsky JC, Baronavsi AP (1999) J Chem Phys 110: 11206
53. Courtney SH, Balk MW, Philips LA, Fleming GR (1988) J Chem. Phys 89: 6697
54. Leitner DM, Wolynes PG (1997) Chem Phys Lett 280: 411
55. Schroeder J, Steinel T, Troe J (2002) J Phys Chem A 106: 5510
56. Hathorn BC, Marcus RA (2000) J Chem Phys 113: 9497
57. Dian BC, Longarte A, Zwier TS (2002) Science 296: 2369
58. Osterheld TH, Brauman JI (1993) J Am Chem Soc 115: 10311
59. Potter ED, Gruebele M, Khundkar LR, Zewail AH (1989) Chem Phys Lett 164: 463
60. Warren WS, Rabitz HS, Dahleh M (1993) Science 259: 1581
61. Makri N (1999) Annu Rev Phys Chem 50: 167
62. Bergt M, Brixner T, Kiefer B, Strehle M, Gerber G (1999) J Phys Chem A 103: 10381
63. Levis RJ, Menkir GM, Rabitz H (2001) Science 292: 709